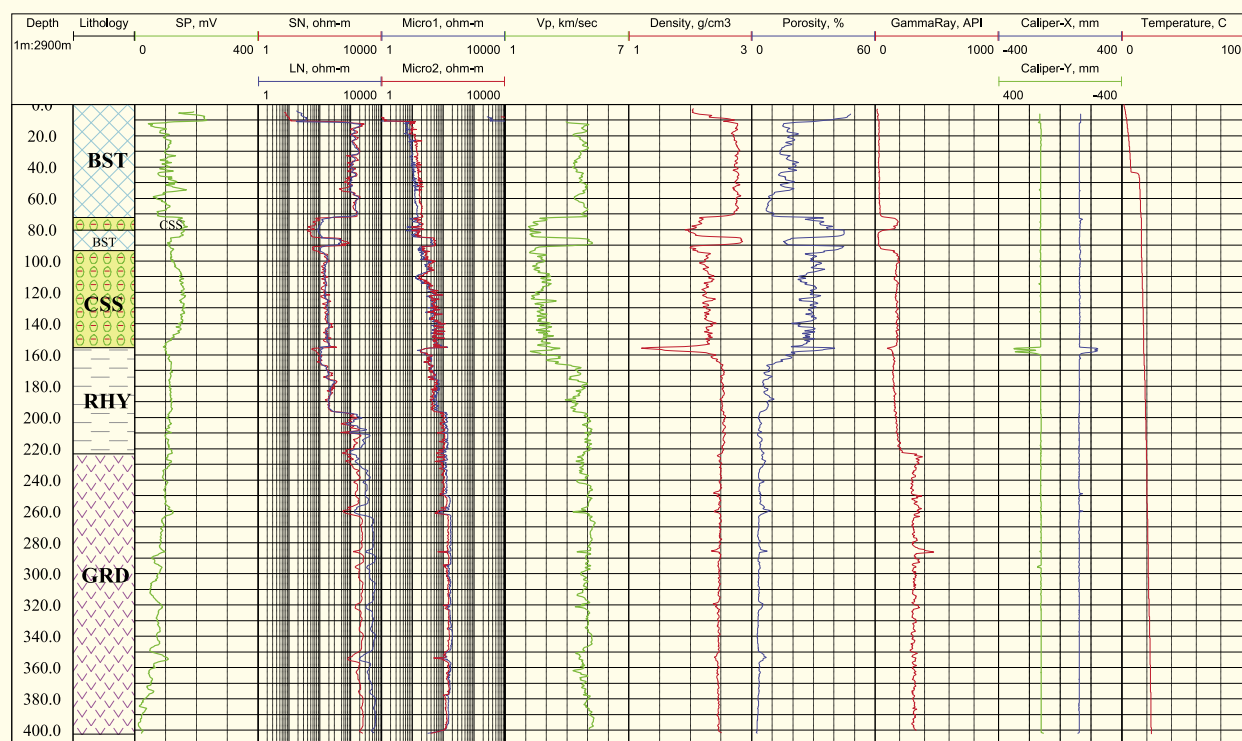


# 防災科学技術研究所による中部日本における孔井検層データ － 活断層，震源域，ヒンジライン －

## Geological and Logging Data of the NIED Boreholes, Japan － Active Fault, Seismogenic Zone, Hingeline －



## Geological and Logging Data of the NIED Boreholes, Japan — Active Fault, Seismogenic Zone, Hingeline —

Tatsuo MATSUDA\*, Kentaro OMURA\*, and Ryuji IKEDA\*\*

*\*Earthquake Reseach Departmant,  
National Research Institute for Earth Science and Disaster Prevention, Japan  
mtastuo@bosai.go.jp, omura@bosai.go.jp*

*\*\*Faculty of Science, Hokkaido University  
ikeryu@mail.sci.hokudai.ac.jp*

### Abstract

The National Research Institute for Earth Science and Disaster Prevention (NIED) has drilled fourteen boreholes in Central Japan, twelve of which (excluding the boreholes at Ashio and Shingu) were drilled as part of the “Active Fault Zone Drilling Project”. Ashio borehole was drilled to examine the stress state, pore water pressure, and heat flow within a seismogenic region, while Shingu borehole was drilled to monitor temporal changes in in situ stress and strain and to reveal their accumulation processes in relation to a great inter-plate earthquake.

In this note, we present geologic columns and geophysical logging data for the boreholes, including spontaneous potential, resistivity, sonic velocity, bulk density, neutron porosity, total gamma ray, spectro-gamma ray, caliper, and temperature. The geophysical data and columns are presented at a scale of 1/2900.

We hope that the data included in this note will contribute to the analysis of the crustal structure of these regions.

**Key words** : Active fault drilling, Geologic column, Geophysical logging, Central Japan

### 1. Introduction

In situ downhole measurements and coring within and around active fault zones are required to gain a better understanding of the structure and material properties of fault rocks and the physical state of active faults and intra-plate crust. In particular, the relationship between stress concentration and the strength heterogeneity of an earthquake fault zone is important in investigating earthquake generation mechanisms.

To understand seismogenesis, it is necessary to compare active faults at different stages of the seismic cycle and under different geophysical and geological conditions; however, there exists little information on the deep structure and continuity of the fault zones associated with active faults. To better understand the structure and environmental conditions of fault zones, NIED carried out the “Active Fault Zone Drilling Project” in Central Japan (Ikeda *et al.*, 1998).

As part of this project, boreholes were drilled through the fault fracture zones of the Nojima fault, which appeared on the surface during the 1995 Great Kobe earthquake (M=7.2), and the Neodani fault, which formed during the 1981 Nobi earthquake (M=8.0), the greatest inland earthquake to have occurred in Japan. A similar investigation focused on the Atera fault, involving surface geophysical surveys and in situ stress measurements within six boreholes drilled around the fault. In this case, resistivity and gravity data obtained from surface geophysical surveys were compared with physical properties determined by borehole logging and measurements of core samples. These results were also compared with in situ stress data derived from hydraulic fracturing within the boreholes (Ikeda, 2001).

In the Ashio area, shallow seismic activity is most active in the Kanto region. We drilled a borehole to 2,000 m depth to access the hypocentral region of these

---

\* Tennodai 3-1, Tsukuba, Ibaraki, 305-0006, Japan

\*\* Kita 10, Nishi 8, Kita-ku, Sapporo, Hokkaido, 060-0810, Japan

earthquakes, and measured the stress state, pore water pressure, and heat flow in the borehole. Our analysis revealed several important characteristics of the stress state within a hypocentral region: very high levels of differential stress occur around the hypocentral region, but these levels show a sharp decline around fracture zones (Tsukahara *et al.*, 1996).

Measurements of crustal stress and strain in deep boreholes are essential when studying subduction-related earthquakes. Especially in the case of earthquakes within the Nankai Trough, it is expected that crustal movements would be detectable even on land, because the focal region associated with subduction of the Philippine Sea plate is located close to land. These basic data, of crustal stress and the physical properties of rocks, were acquired by drilling to a depth of 550 m at Shingu City, Wakayama prefecture, on the Kii Peninsula. In situ experiments were conducted within the borehole, including measurements of crustal stress using the hydraulic fracturing method. We also used an intelligent strain meter to measure in situ stress, via the over-coring method, at depths greater than 500 m. The final goal of this study was to monitor temporal changes in in situ stress and strain, and to reveal their accumulation processes in relation to a great inter-plate earthquake (Ikeda *et al.*, 2001).

## 2. Locations of the NIED boreholes

**Fig. 1** shows locations of drilling sites in Central Japan. **Table 1** shows the latitude, longitude (International Terrestrial Reference Frame), and elevation of each borehole, while **Fig. 2** shows the Atera fault system and locations of drilling sites in the Atera area. **Fig. 3 – 15** show the location of each borehole plotted on a 1:25,000 topographic map published by the Geographical Survey Institute of Japan.

## 3. Geophysical logging items and method

### 3.1 List of the geophysical logging items

**Table 2** lists the geophysical logging items measured in the boreholes.

### 3.2 Methods employed in measuring the geophysical logging items (SPWLA, 1984; Chapellier, 1992; Hearst, 2000)

#### 3.2.1 Spontaneous potential log: SP (spontaneous potential, mV)

An SP log measures the difference in electrical potential between an electrode moving along the borehole and a reference electrode fixed at the surface. SP arises mainly from electrochemical effects when fluids of contrasting salinities are encountered, such as drilling mud and water within the rock around the borehole through which the log

is passing. An SP log is useful in examining the distribution of porous and permeable/impermeable zones in the drilled rock.

#### 3.2.2 Electrical log: SN (short normal, ohm-m); LN (long normal, ohm-m); Micro1 (micro log 1 inch, ohm-m); Micro2 (micro log 2 inch, ohm-m); MG (medium guard, ohm-m)

An electrical log measures the resistivity of the rocks around the borehole. Various types of tools can be used, each with different configurations of electrodes. For a normal log, a current electrode and potential electrode are configured on the tool. Potential difference is measured between the potential electrode and a reference electrode at the surface while a constant current passes between the current electrode and the surface electrode. Because the electrodes on the surface are situated in an ‘infinite’ space, the measured potential difference depends on the characteristics of the rock around the current and potential electrodes on the tool. The distances between the two electrodes are 25 cm (short normal) or 100 cm (long normal).

For a micro log, the resistivity is measured by a simple array of three button electrodes at 1-inch spacings on a pad pressed against the borehole wall. The current electrode occupies the lowermost position. The potential of the uppermost electrode with respect to a remote reference electrode yields 2-inch normal resistivity. At the same time, the potential difference between the upper two electrodes gives 1-inch lateral resistivity. The micro log consists of two resistivity curves that are expected to coincide with each other in the absence of mud cake on the borehole wall.

A guard log is a type of focused log. A central current electrode is placed between upper and lower supplementary guard electrodes. A controlled current is transmitted from the guard electrodes to maintain them at the same potential such that the current from the central electrode flows in a thin horizontal layer at an angle of 90 degrees to the tool. Apparent resistivity is obtained by measuring the potential of the central electrode. The employed focusing technique means that the guard log is advantageous in obtaining the fine structure of thin beds in the rock around the borehole.

#### 3.2.3 Sonic log: V<sub>p</sub> (P wave velocity, km/sec); V<sub>s</sub> (S wave velocity, km/sec)

A sonic log is an acoustic log that measures the interval transit time of compressive and shear waves in the rock around the borehole. There are one transmitter and two receivers on the tool. The tool measures directly the travel time from transmitter to receiver, comprising the travel time through mud located between the transmitter and the

borehole wall, between the borehole wall and the receiver, and through the wall rock along the same distance as that between the transmitter and receiver. The difference between the two travel times represents the travel time through the wall rock along the fixed distance between the two receivers, generally a distance of 1 foot. The difference in travel time represents the interval transit time, which is converted to the acoustic velocity of the rock around the borehole.

### 3.2.4 Formation density log (sometimes called a gamma-gamma log): Density (density, g/cm<sup>3</sup>)

A formation density log measures the intensity of backscattered gamma rays from the rock around the borehole using a detector mounted in the tool and shielded from a gamma ray source (e.g., <sup>137</sup>Cs). The intensity of backscattered gamma rays depends on the electron density, which is closely related to the bulk density of the rock around the borehole. The intensity of the backscattered gamma rays is converted to rock density using a calibration curve.

### 3.2.5 Neutron (Porosity) log: Porosity (porosity, %)

A neutron log counts the neutrons emitted from a neutron source installed within the tool and scattered by the rock around the borehole. Fast neutrons continuously emitted from the source (a radioisotope of Am-Be) are slowed by collisions with atomic nuclei within the rock around the borehole, thereby becoming low-energy thermal neutrons that are captured by the neutron detector. Because collisions with hydrogen atoms — which have similar masses to the neutrons — are by far the most effective in terms of slowing the neutrons, the number of neutrons recorded by the detector is inversely proportional to the concentration of hydrogen in the rock around the borehole. In water-saturated rock, the hydrogen content is equivalent to the pore water content, i.e., porosity. The porosity is derived from the number of detected neutrons via an empirically determined relationship.

### 3.2.6 Gamma-ray log: GammaRay (gamma- ray, API)

A gamma-ray log counts all of the gamma rays, without energy discrimination, radiated from natural radioactive isotopes in the rock around the borehole, being mainly uranium (<sup>238</sup>U), thorium (<sup>232</sup>Th), and potassium (<sup>40</sup>K). The API (American Petroleum Institute) unit for radioactivity is employed, based on an artificial radioactive concrete block housed in the API calibration facility at the University of Houston, Texas, USA.

### 3.2.7 Spectral gamma-ray log. K (potassium, %) ; U (uranium, ppm) ; Th (thorium, ppm)

A spectral gamma-ray log counts gamma rays at specific energy levels radiated from radioactive isotopes in the rock around the borehole. The isotope species and

element concentrations can be determined once the specific energy levels and amounts of gamma rays at the specific energy levels (API unit) are known.

### 3.2.8 Caliper log: Caliper-X (caliper x-axis, mm); Caliper-Y (caliper y-axis, mm)

A caliper log measures the borehole diameter. The tool has one or more arms that are extended mechanically and placed in contact with the borehole wall. The degree of extension of the arm(s) is converted to the length from the center of the tool to the borehole wall.

### 3.2.9 Temperature log: Temperature (temperature, °C)

A temperature log measures temperature within the borehole using a thermistor sensor installed within the tool such that fluid passes over the sensor as the tool travels down the borehole.

## 4. Legend of the geologic columns

Abbreviations in the geologic columns are as follows.

ADM	: adamellite
AND	: andesite
BRE	: breccia
BST	: basalt
CHT	: chert
CMS	: conglomerate and mudstone
CSS	: conglomerate and sandstone
FRZ	: fracture zone
GCG	: granitic conglomerate
GRD	: granodiorite
PHT	: porphyrite
RHY	: rhyolite
SCG	: sandy conglomerate
SLT	: slate
SMA	: sandstone and mudstone alternation
SMS	: sandy mudstone
TNT	: tonalite

## 5. Geologic column and geophysical logs of the NIED boreholes

Geophysical logs for the NIED boreholes are shown in **Figs. 16 – 29** alongside geological columns. Logs were compiled for various rock types. Broadly speaking, we found correlations among electrical, sonic, density, and neutron logs, while gamma-ray logs discriminate different rock types. Some of the log items show drastic changes within fracture zones relative to values in adjacent host rocks, irrespective of rock type. These findings suggest that the logging data presented in this note will contribute to studies of crustal structure and petrophysics.

### Acknowledgements

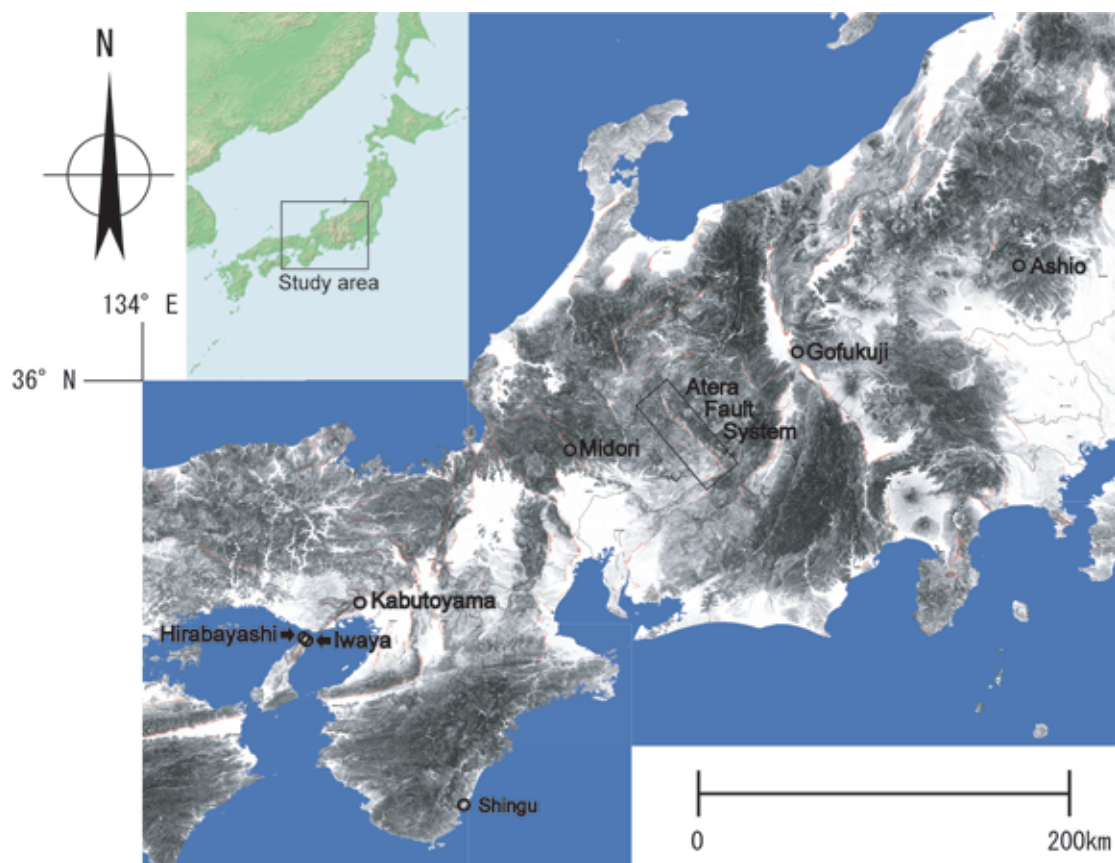
We would like to thank the staff of Geophysical

Surveying Co., Ltd. and Sumiko Consultants Co., Ltd. involved in the measurements.

#### References

- 1) Chapellier, D. (1992): Well logging in hydrogeology, 175 pp., A.A. Balkema Pub., Brookfield.
- 2) Hearst, J. R., Nelson, P. H., and Paillett, F. L. (2000): Well logging for physical properties, second ed., 483 pp, John Wiley & Sons Ltd., West Sussex.
- 3) Ikeda, R., Omura, K., and Iio, Y. (1998): Stress measurements around active fault. *Earth Monthly*, **21**, 91-96. (in Japanese)
- 4) Ikeda, R., (2001): Outline of the fault zone drilling project by NIED in the vicinity of the 1995 Hyogo-ken Nanbu earthquake, Japan. *The Island Arc*, **10**-3/4, 199-205.
- 5) Ikeda, R., Omura, K., Iio, Y., Ishii, H., Kobayashi, Y., Nishigami, K., and Yamauchi, T. (2001): Crustal stress and strain measurements on land for studying the Nankai trough earthquake. *Journal of geography*, **110**, 544-556.
- 6) SPWLA (1984): Glossary of terms & expressions used in well logging, second ed., 116 pp., Society of Professional Well Log Analysts, Houston.
- 7) Tsukahara, H., Ikeda, R., and Omura, K. (1996): In-situ stress measurements in an earthquake focal area, *Tectonophysics*, **262**, 281-290.

(Accepted : February 5, 2008)


**Fig. 1** Locations of the drilling sites in central Japan.

**Table 1** Location data of the boreholes (International Terrestrial Reference Frame) .

Site name	Latitude, °	'	''	Longitude °	'	''	Elevation, m	Address
Ashio	36	37	5.9	139	23	59.4	642	3658, 3596, Ashio, Nikko, Tochigi pref.
	36.61831			139.39983				
Tsukechi	35	38	15.3	137	27	22	495	Nakano, Tsukechi, Nakatsugawa, Gifu pref.
	35.63758			137.45611				
Kawaue	35	36	32.5	137	29	49.9	460	Kawaue, Nakatsugawa, Gifu pref.
	35.60903			137.49719				
Fukuoka	35	34	35.5	137	27	57.2	383	Fukuoka, Nakatsugawa, Gifu pref.
	35.57653			137.46589				
Hatajiri	35	33	35.7	137	26	47	305	1605-1-2, Fukuoka, Nakatsugawa, Gifu pref.
	35.55992			137.44639				
Ueno	35	35	47.8	137	29	1.4	526	245-2, 3, Ueno, Nakatsugawa, Gifu pref.
	35.59661			137.48372				
Hagiwara	35	56	14.2	137	11	32.5	509	1943-3, Ozaki, Hagiwara, Gifu pref.
	35.93728			137.19236				
Gofukuji	36	10	9.1	138	0	9	783	Gofukuji, Uchida, Matsumoto, Nagano pref.
	36.16919			138.00250				
Midori	35	36	51.7	136	37	13.9	160	Neomidori, Motosu, Gifu pref.
	35.61436			136.62053				
Hirabayashi	34	34	54.6	134	58	13.7	65	Nojimahirabayashi, Awaji, Hyogo pref.
	34.58183			134.97047				
Iwaya	34	35	26.9	135	0	3.3	120	Iwaya, Awaji, Hyogo pref.
	34.59081			135.00092				
Kabutoyama	34	46	27.7	135	19	32.7	222	Kabutoyama, Nishinomiya, Hyogo pref.
	34.77436			135.32575				
Shingu	33	41	19.4	135	58	6.8	24	1510, Sano, Shingu, Wakayama pref.
	33.68872			135.96856				

**Table 2** List of the geophysical logging items in the boreholes.

Site name	SP (mV)	SN (ohm-m)	LN (ohm-m)	Micro1 (ohm-m)	Micro2 (ohm-m)	MG (ohm-m)	Vp (km/sec)	Vs (km/sec)	Density (g/cm <sup>3</sup> )	Porosity (%)	GammaRay (API)	Caliper-X (mm)	Caliper-Y (mm)	Temperature (°C)	K (%)	U (ppm)	Th (ppm)
Ashio	○	○	○	○	○		○		○	○	○	○	○	○	○	○	○
Tsukechi											○			○			
Kawaue	○	○	○	○	○		○	○	○	○	○	○	○	○			
Fukuoka	○	○	○						○	○	○	○	○	○			
Hatajiri	○	○	○				○	○	○	○				○			
Ueno	○	○	○	○	○		○	○	○	○	○	○	○	○			
Hagiwara	○	○	○			○	○		○	○	○	○	○	○			
Gofukuji	○	○	○						○	○	○	○	○	○			
Midori (vertical)	○	○	○	○	○				○	○	○	○	○	○	○	○	○
Midori (inclined)	○	○	○	○	○				○	○	○	○	○	○			
Hirabayashi	○	○	○	○	○				○	○	○	○	○	○			
Iwaya	○	○	○	○	○				○	○	○	○	○	○			
Kabutoyama	○	○	○	○	○				○	○	○	○	○	○			
Shingu	○	○	○	○	○			○	○	○	○	○	○	○			

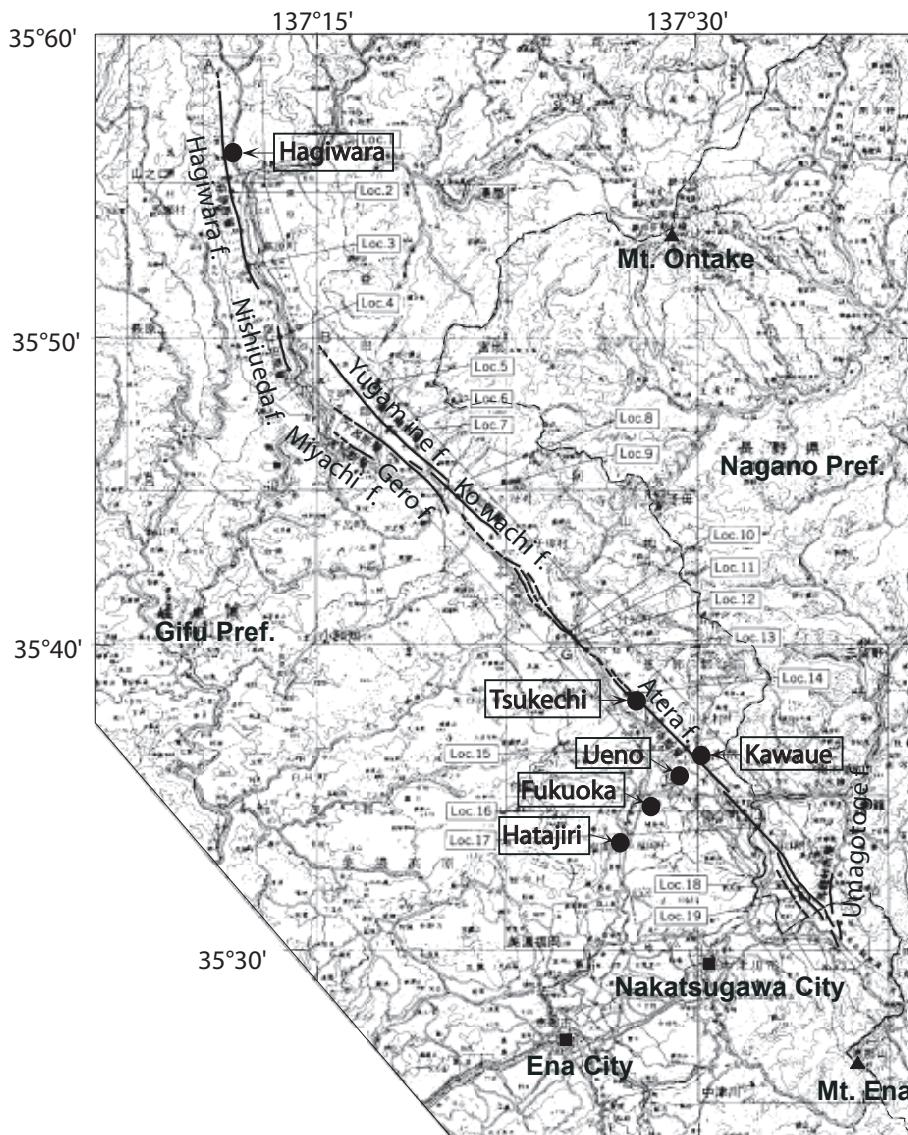


**Fig. 2** Atera fault system and the locations of drilling sites (from Strip Map of the Atera Fault System, Geological Survey, Japan, 1993).

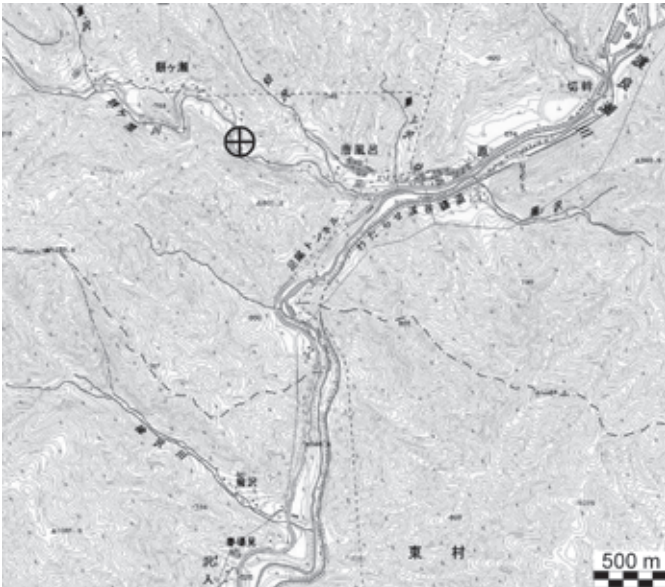


**Fig. 3** Location of the Ashio borehole plotted on a 1:25,000 topographic map of Ashio published by the Geographical Survey Institute of Japan.



**Fig. 4** Location of the Tsukechi borehole plotted on a 1:25,000 topographic map of Tsukechi published by the Geographical Survey Institute of Japan.



**Fig. 5** Location of the Kawaue borehole plotted on a 1:25,000 topographic map of Tsukechi published by the Geographical Survey Institute of Japan.

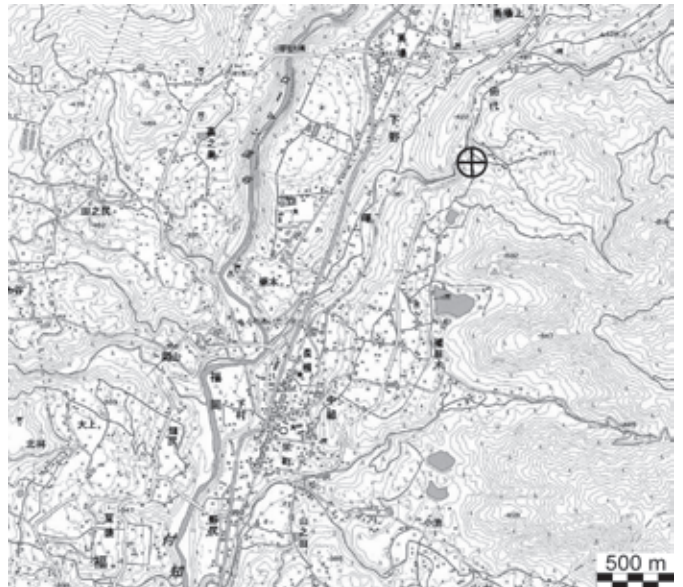


**Fig. 6** Location of the Fukuoka borehole plotted on a 1:25,000 topographic map of Minofukuoka published by the Geographical Survey Institute of Japan.



**Fig. 7** Location of the Hatajiri borehole plotted on a 1:25,000 topographic map of Minofukuoka published by the Geographical Survey Institute of



**Fig. 8** Location of the Ueno borehole plotted on a 1:25,000 topographic map of Tsukechi published by the Geographical Survey Institute of Japan.

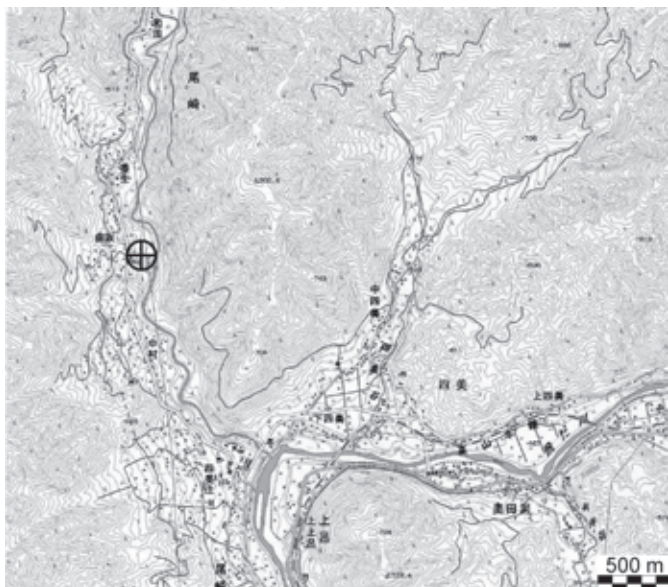


**Fig. 9** Location of the Hagiwara borehole plotted on a 1:25,000 topographic map of Yamanokuchi published by the Geographical Survey Institute of Japan.



**Fig. 10** Location of the Gofukuji borehole plotted on a 1:25,000 topographic map of Yamabe published by the Geographical Survey Institute of Japan.

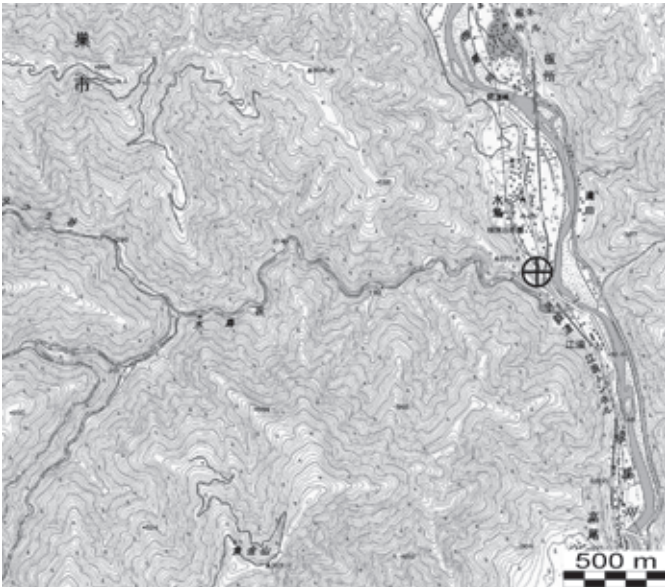


**Fig. 11** Location of the Midori borehole plotted on a 1:25,000 topographic map of Tarumi published by the Geographical Survey Institute of Japan.



**Fig. 12** Location of the Hirabayashi borehole plotted on a 1:25,000 topographic map of Kariya published by the Geographical Survey Institute of Japan.



**Fig. 13** Location of the Iwaya borehole plotted on a 1:25,000 topographic map of Suma published by the Geographical Survey Institute of Japan.



**Fig. 14** Location of the Kabutoyama borehole plotted on a 1:25,000 topographic map of Takarazuka published by the Geographical Survey Institute of Japan.



**Fig. 15** Location of the Shingu borehole plotted on a 1:25,000 topographic map of Shingu published by the Geographical Survey Institute of Japan.

## 防災科学技術研究所による中部日本における孔井検層データ —活断層，震源域，ヒンジライン—

松田達生\*・小村健太郎\*・池田隆司\*\*

\*独立行政法人 防災科学技術研究所 地震研究部

\*\*北海道大学大学院 理学研究院

### 要 旨

独立行政法人防災科学技術研究所は日本中部において14井の掘削を行った。そのうち、足尾及び新宮を除く12井は、同研究所による「活断層掘削プロジェクト」によるものである。足尾は、同地域周辺が関東地方でも浅い地震活動が最も活発なことから、その震源域まで到達する深さ2,000 mの掘削井において応力状態、間隙水圧、熱流量などを主に測定した。新宮は、南海地震のような海溝型巨大地震における応力等の蓄積の仕方を調べるために、孔井内の原位置測定によるモニタリングを目的としたものである。本研究資料では、これらの研究を行う上での基礎データとなる各孔井の地質柱状図及び各種物理検層データをまとめた。

**キーワード**：活断層ドリリング，地質柱状図，物理検層，中部日本

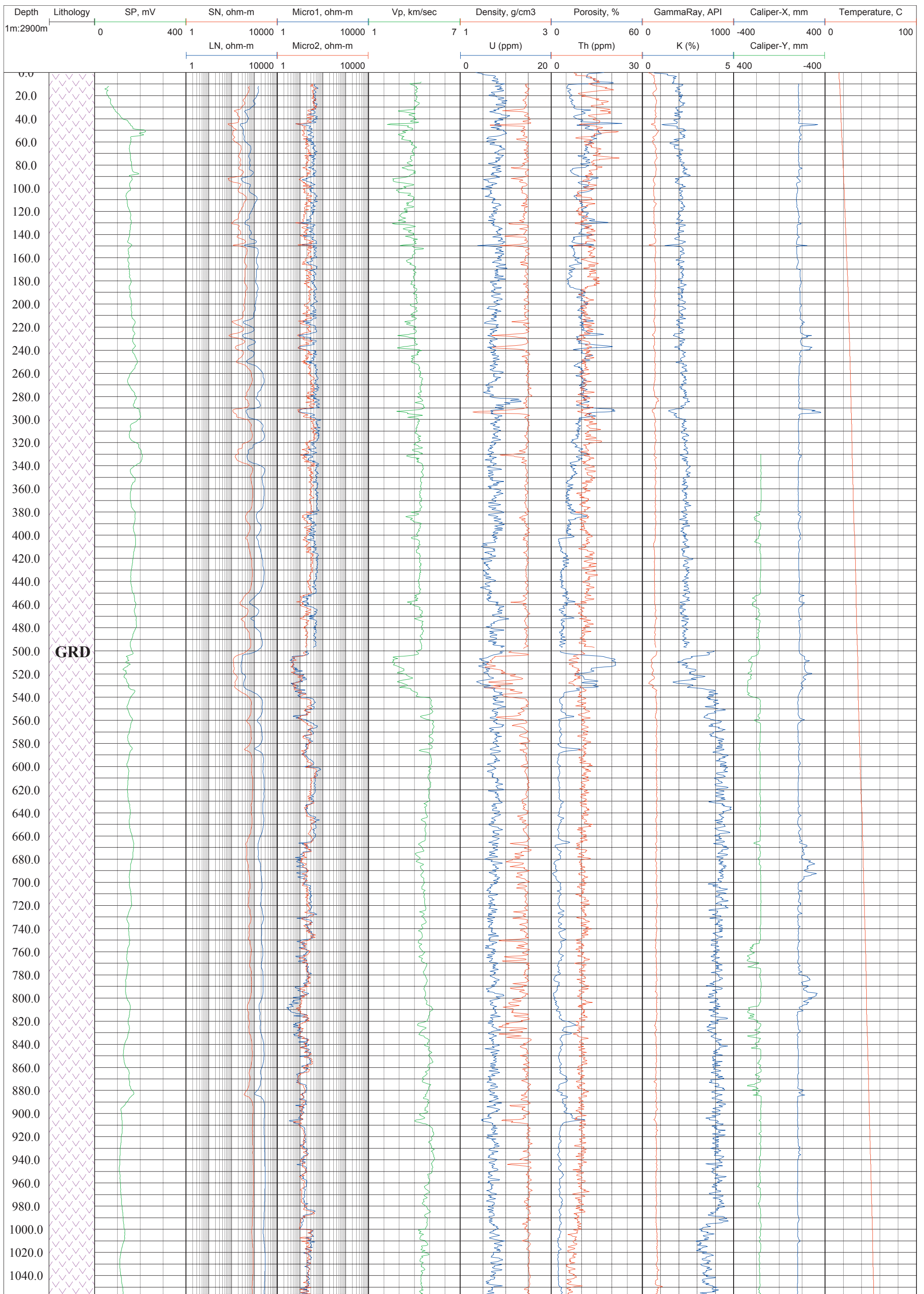


Fig. 16 Geologic column and geophysical logging charts of the Ashio borehole.

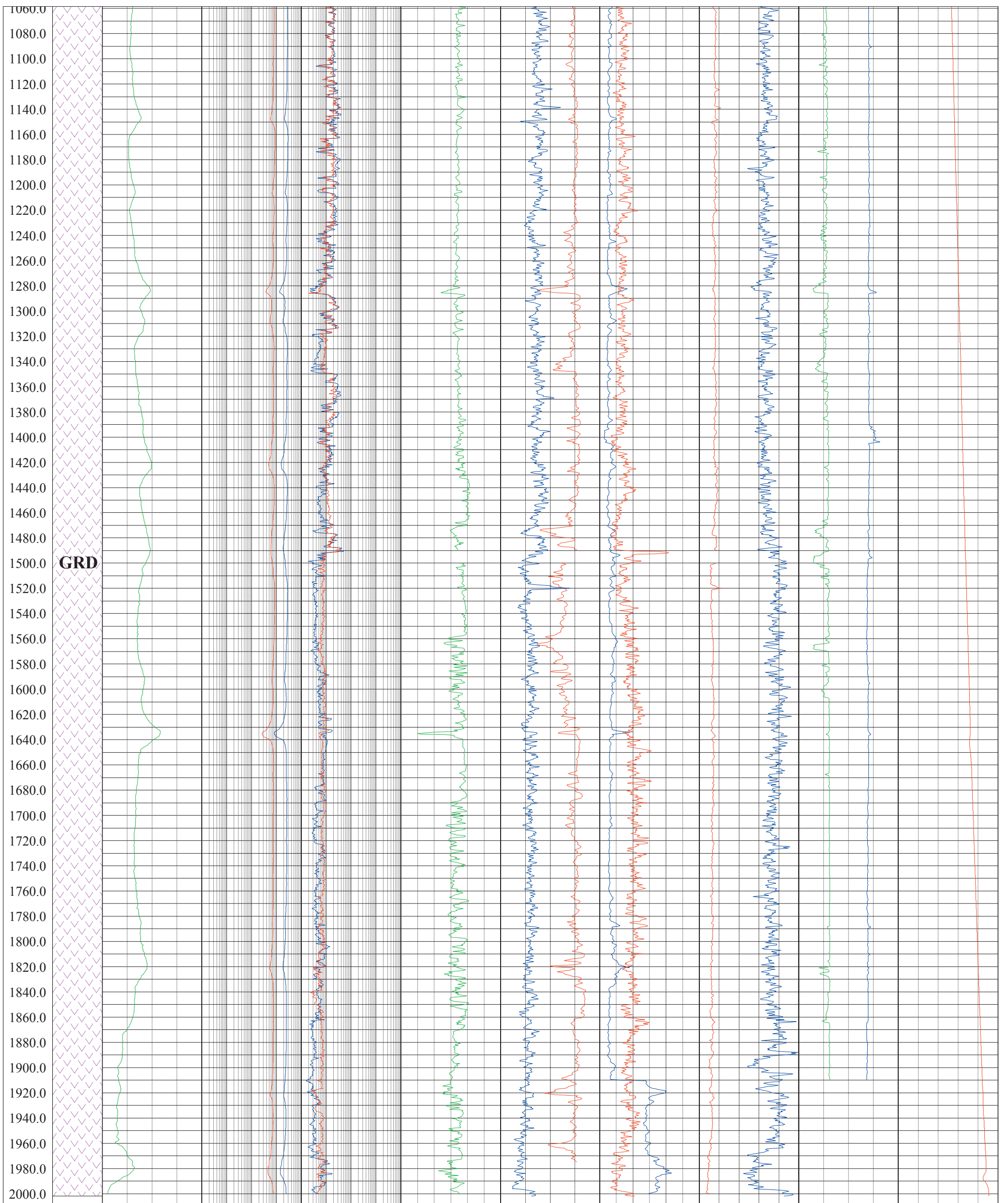


Fig. 16 Geologic column and geophysical logging charts of the Ashio borehole (continued).

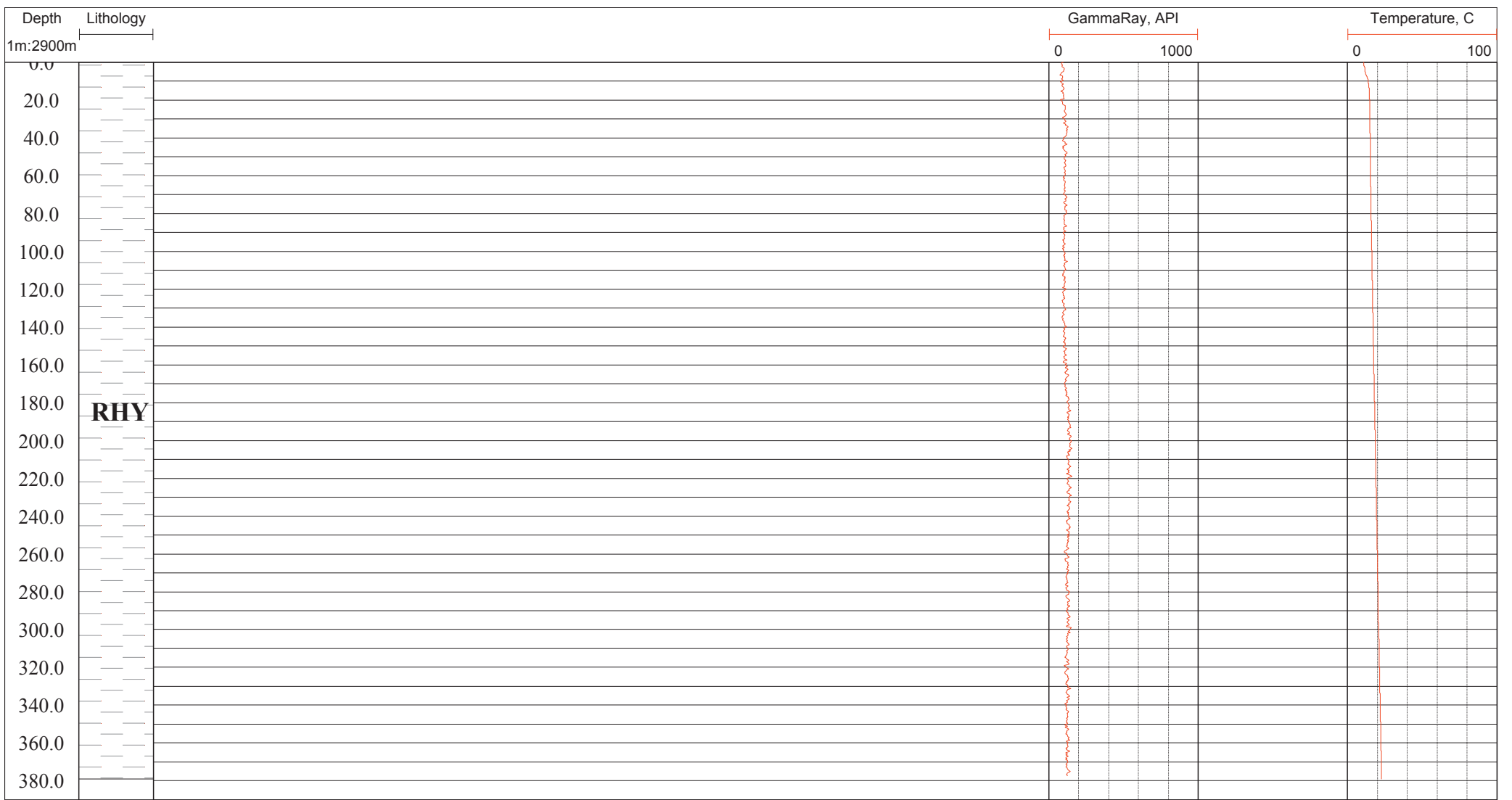


Fig. 17 Geologic column and geophysical logs for the Tsukechi borehole.

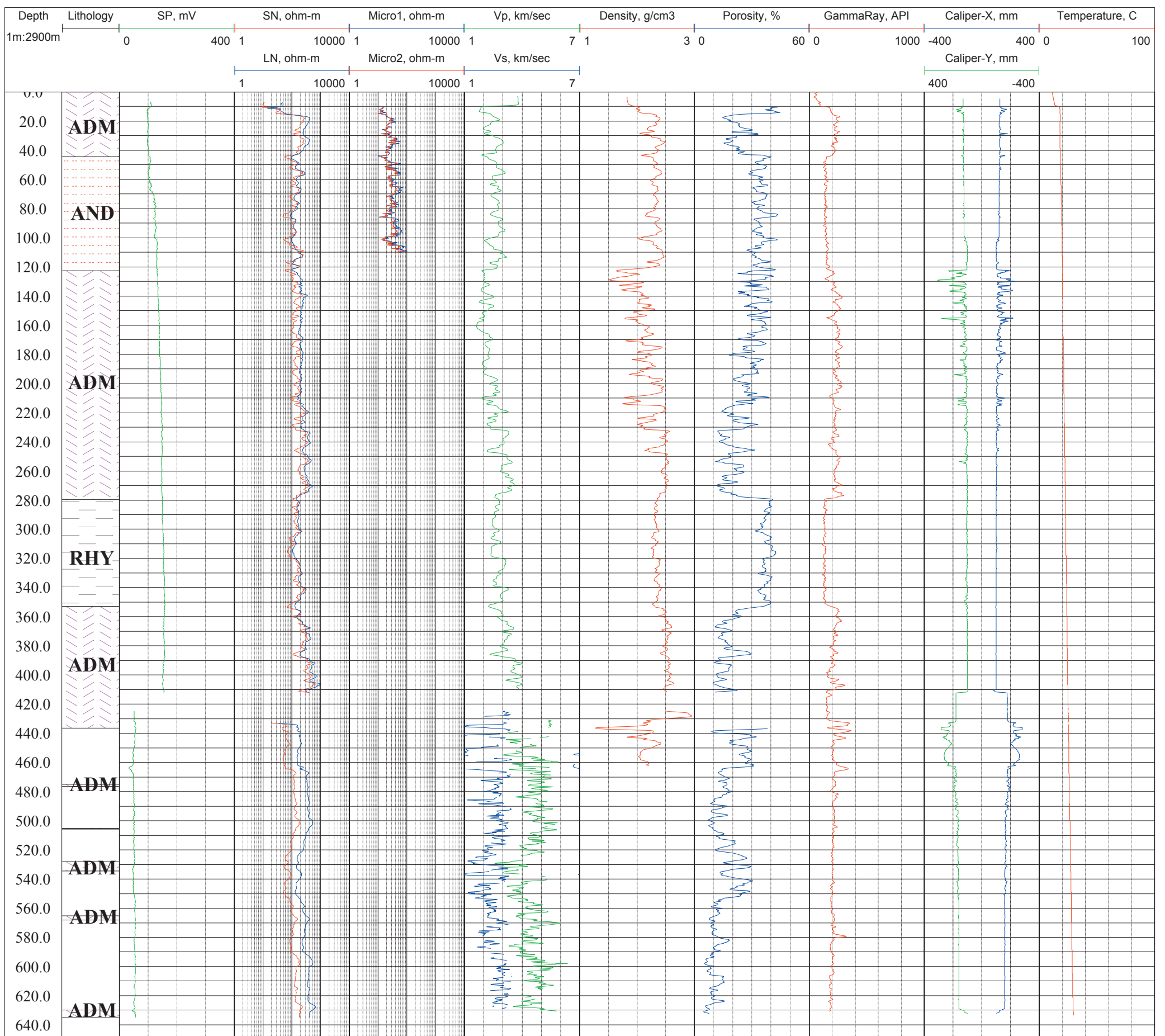


Fig. 18 Geologic column and geophysical logs for the Kawaue borehole

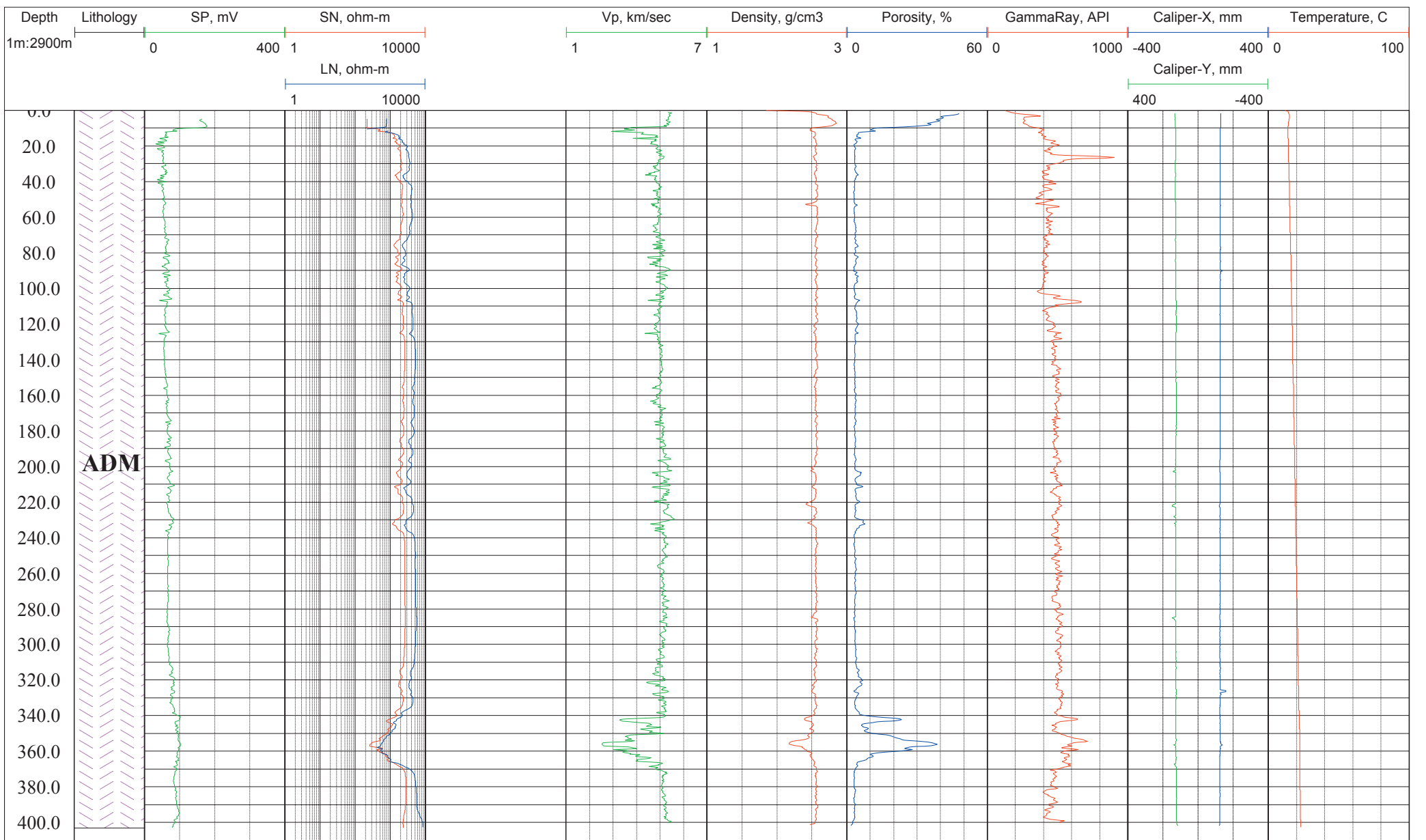


Fig. 19 Geologic column and geophysical logs for the Fukuoka borehole.

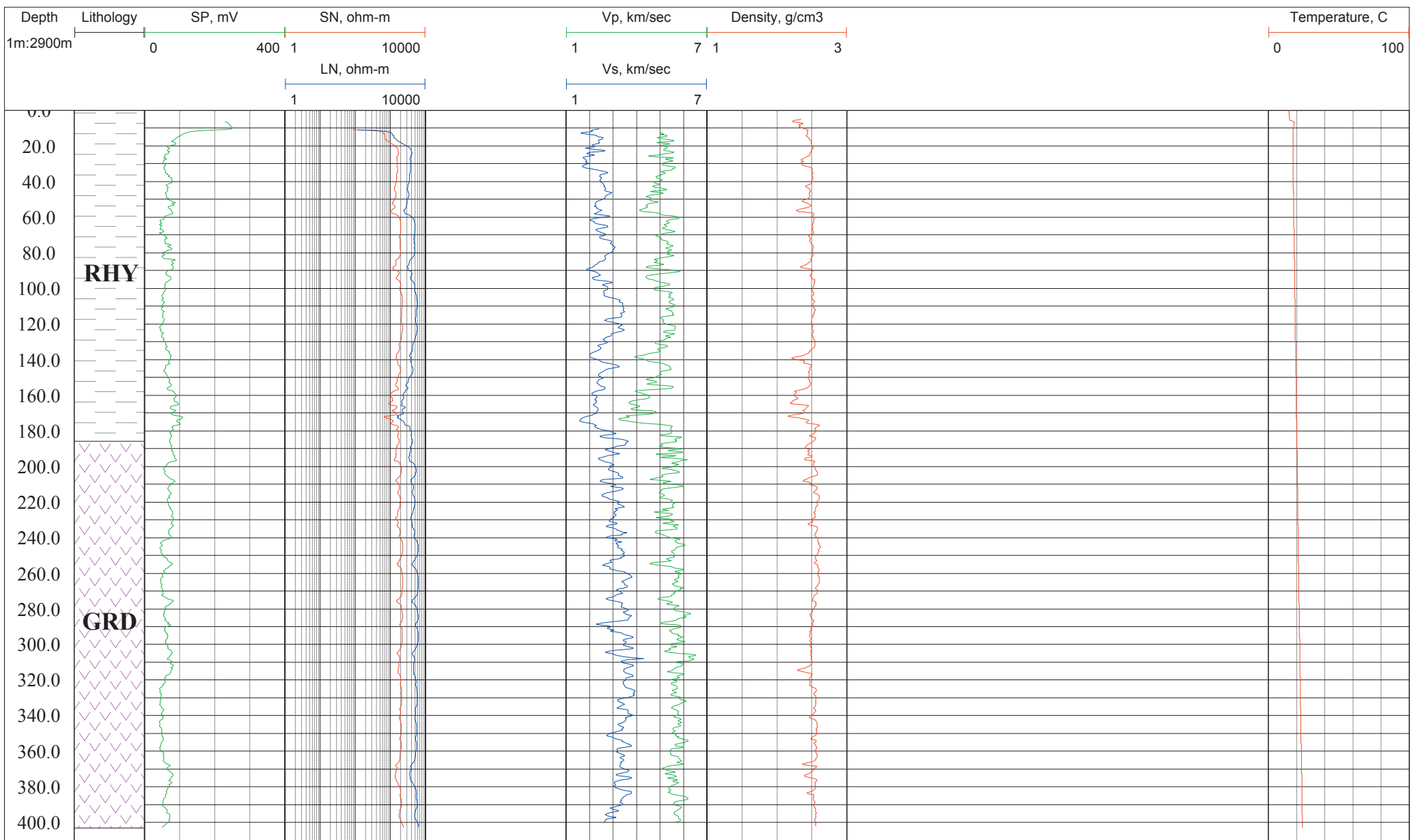


Fig. 20 Geologic column and geophysical logs for the Hatajiri borehole.

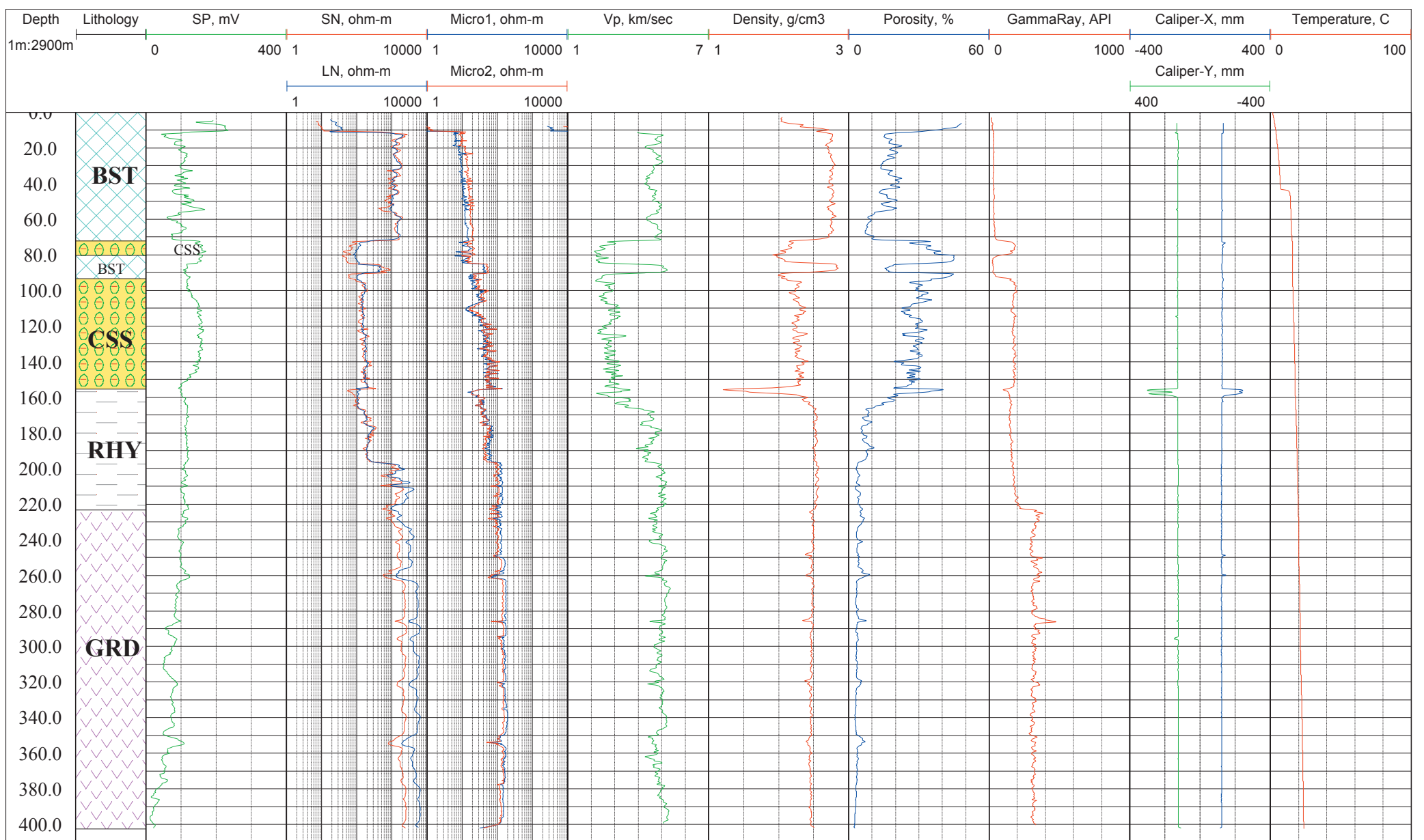


Fig. 21 Geologic column and geophysical logs for the Ueno borehole.

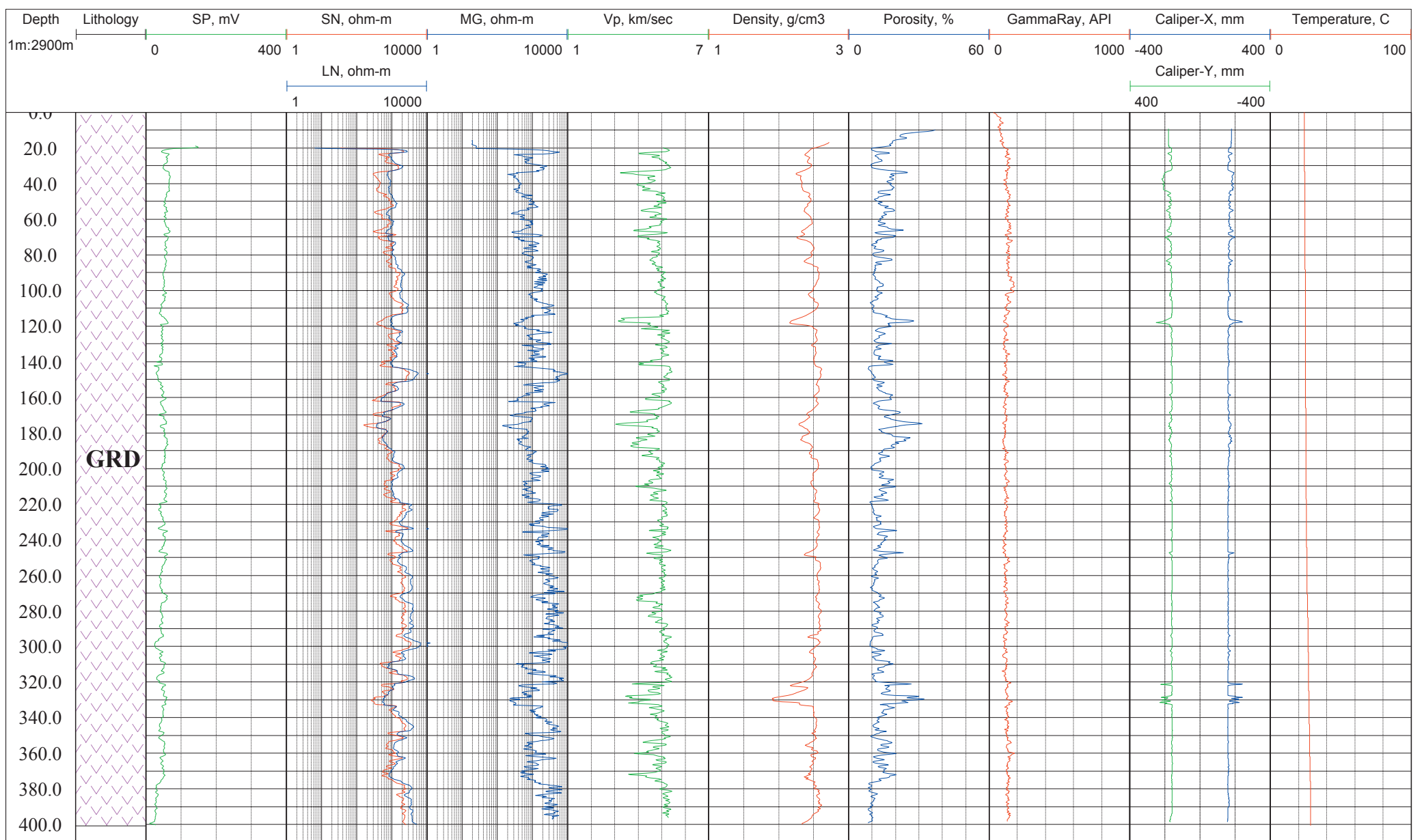


Fig. 22 Geologic column and geophysical logs for the Hagiwara borehole.

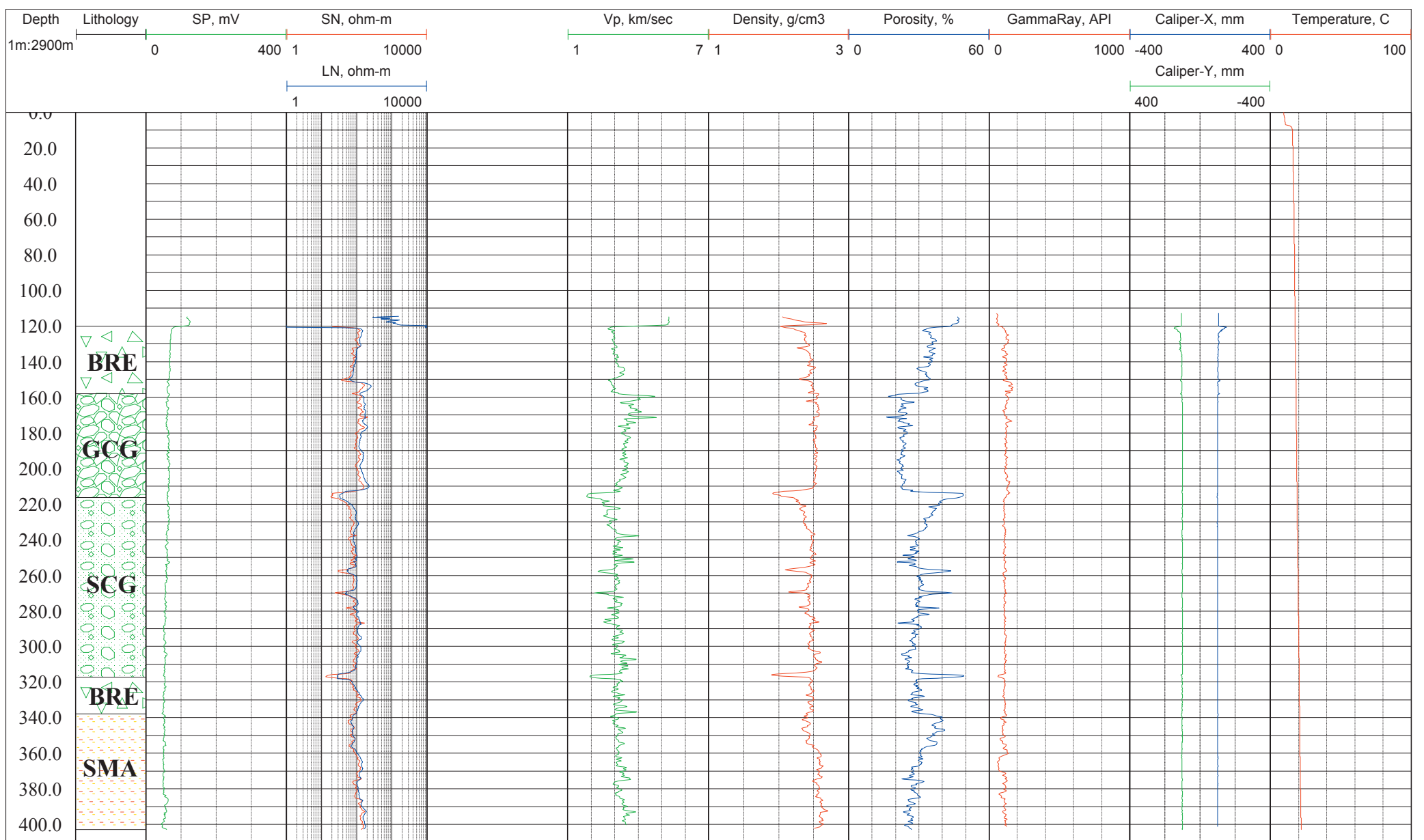


Fig. 23 Geologic column and geophysical logs for the Gofukuji borehole.

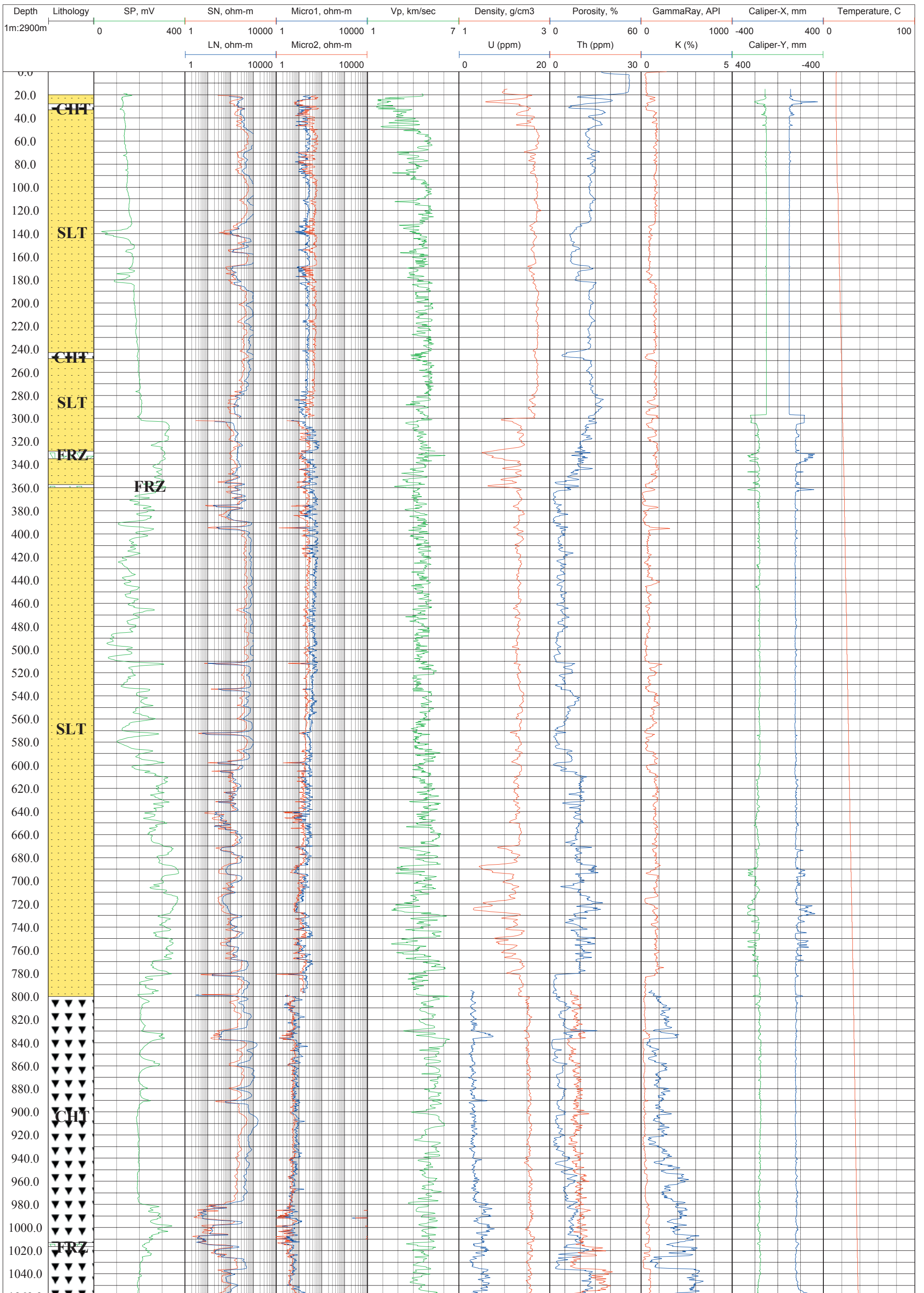


Fig. 24 Geologic column and geophysical logs for the Midori (vertical) borehole.

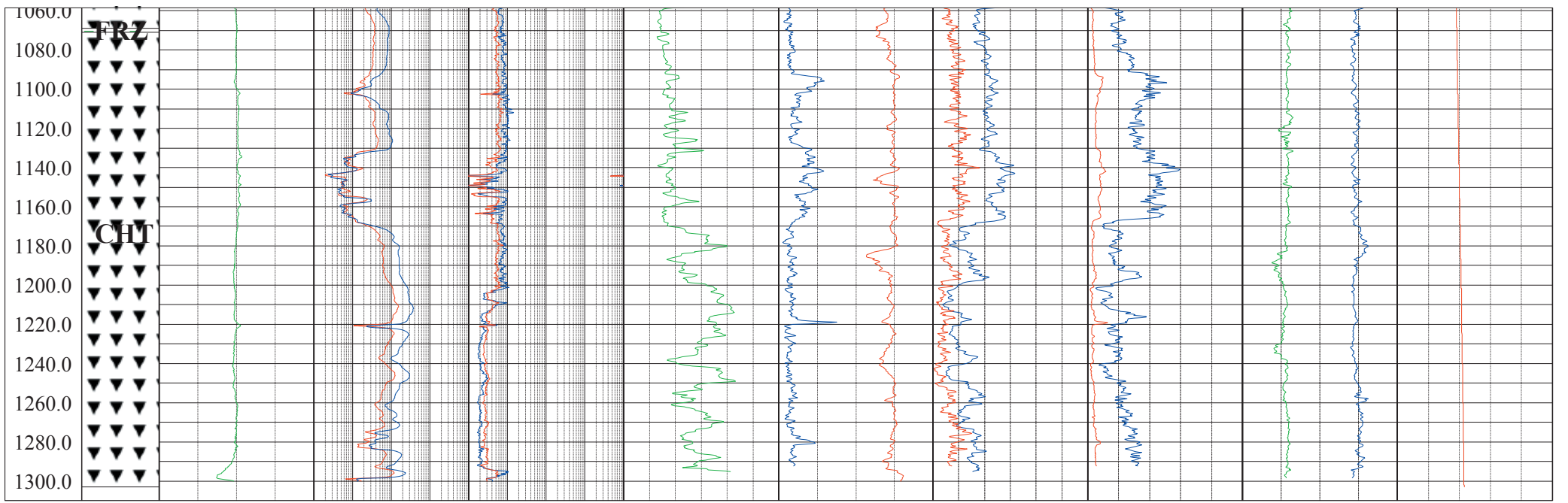


Fig. 24 Geologic column and geophysical logs for the Midori (vertical) borehole (continued).

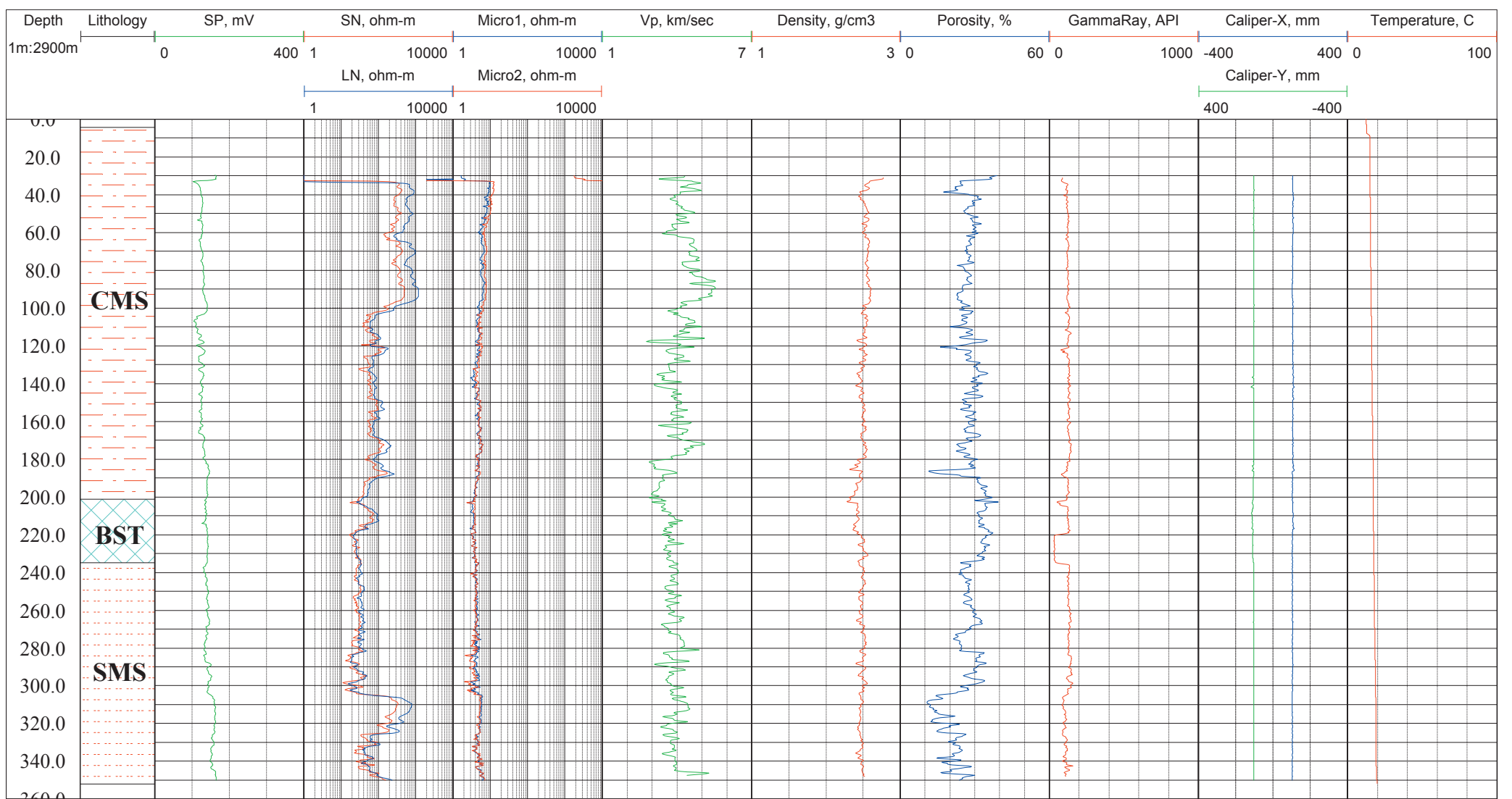


Fig. 25 Geological column and geophysical logs for the Midori (inclined) borehole.

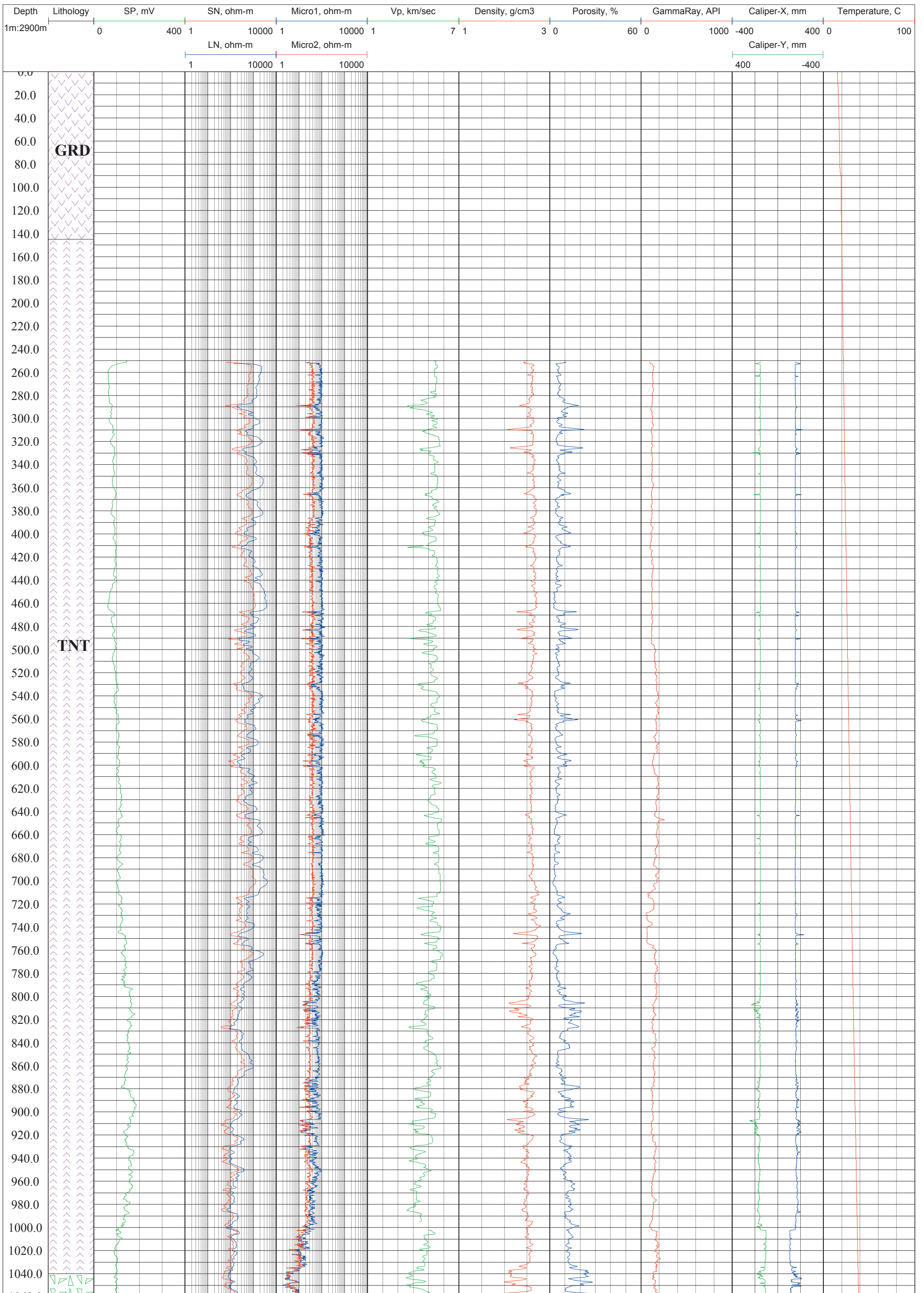


Fig. 26 Geologic column and geophysical logs for the Hirabayashi borehole.

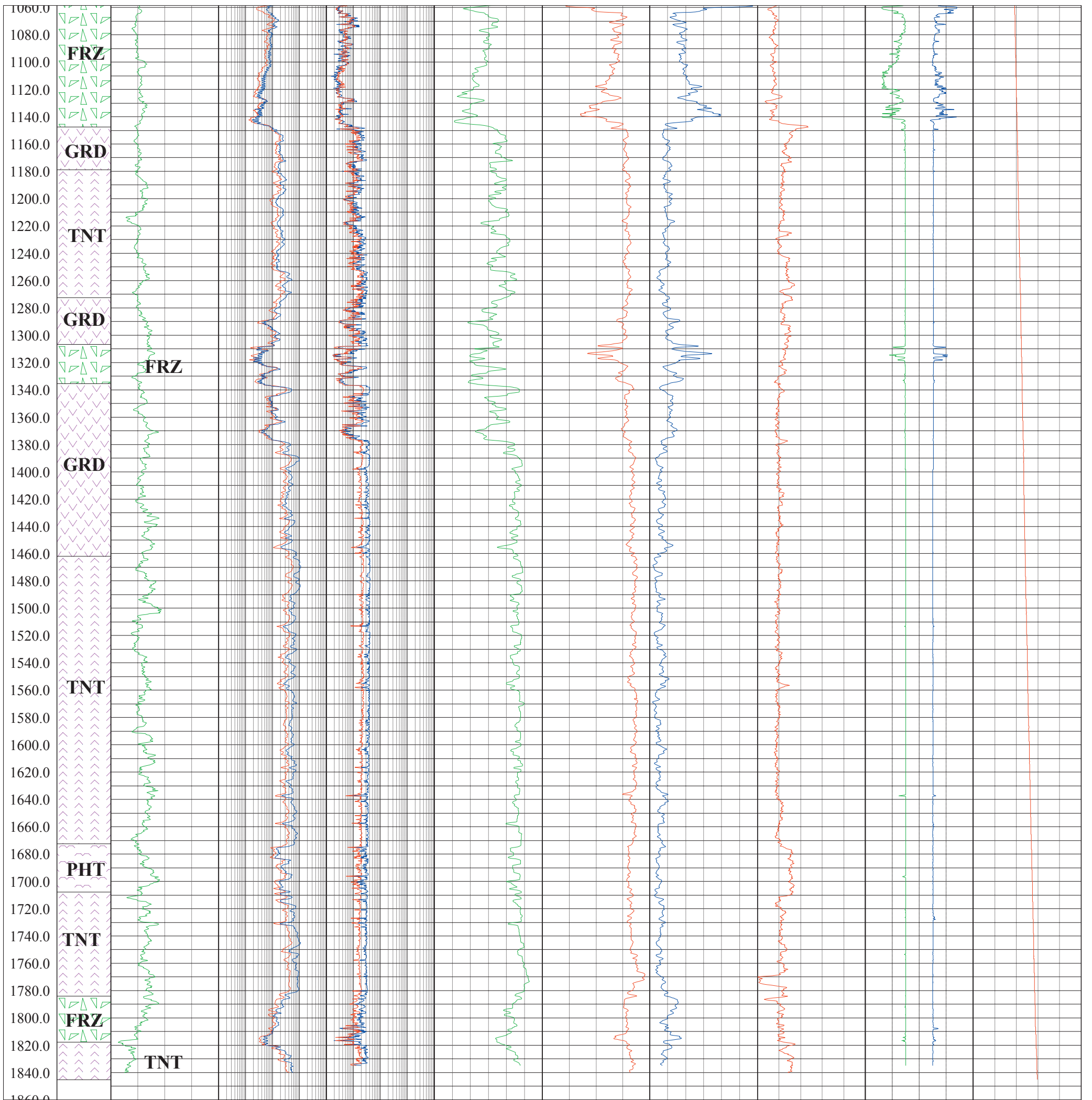


Fig. 26 Geologic column and geophysical logs for the Hirabayashi borehole (continued).

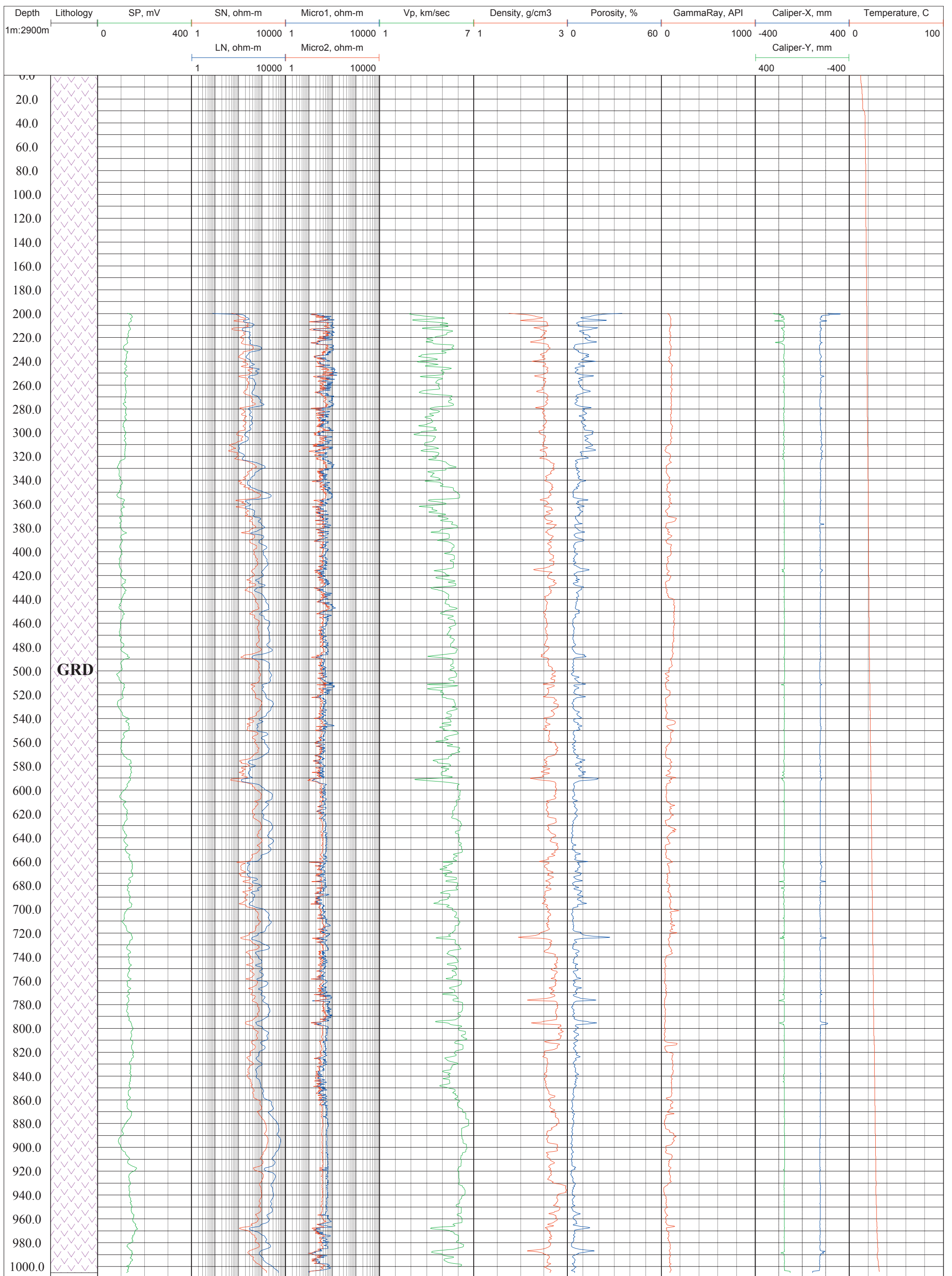


Fig. 27 Geologic column and geophysical logs for the Iwaya borehole.

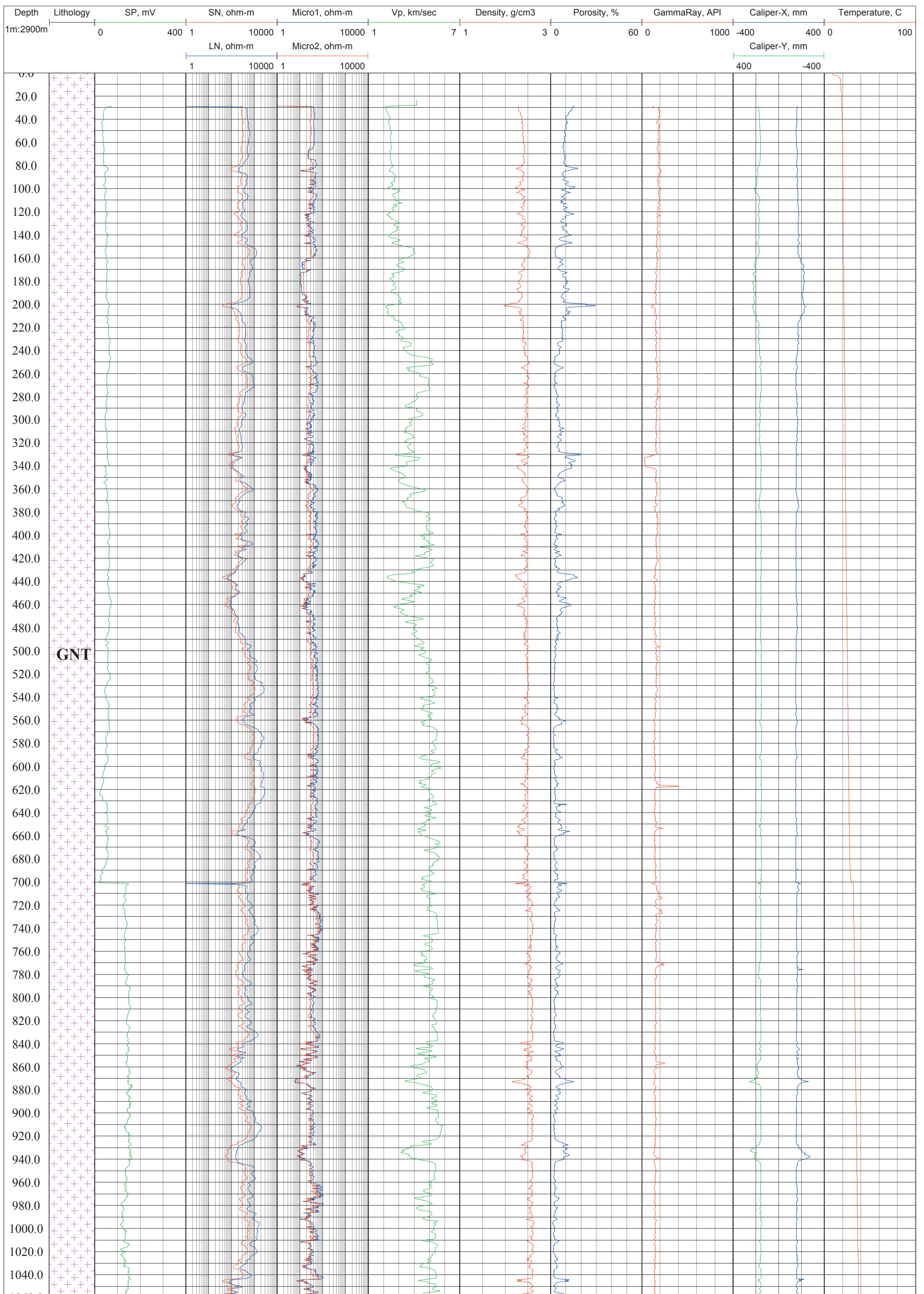


Fig. 28 Geologic column and geophysical logs for the Kabutoyama borehole.

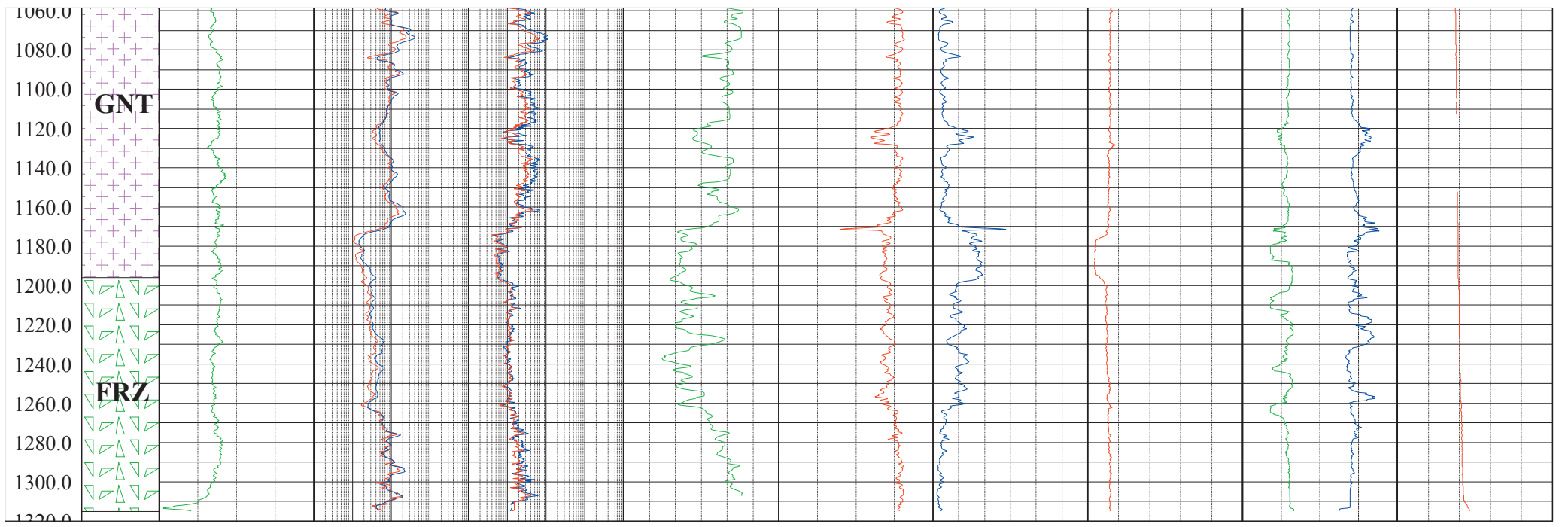


Fig. 28 Geologic column and geophysical logs for the Kabutoyama borehole (continued).

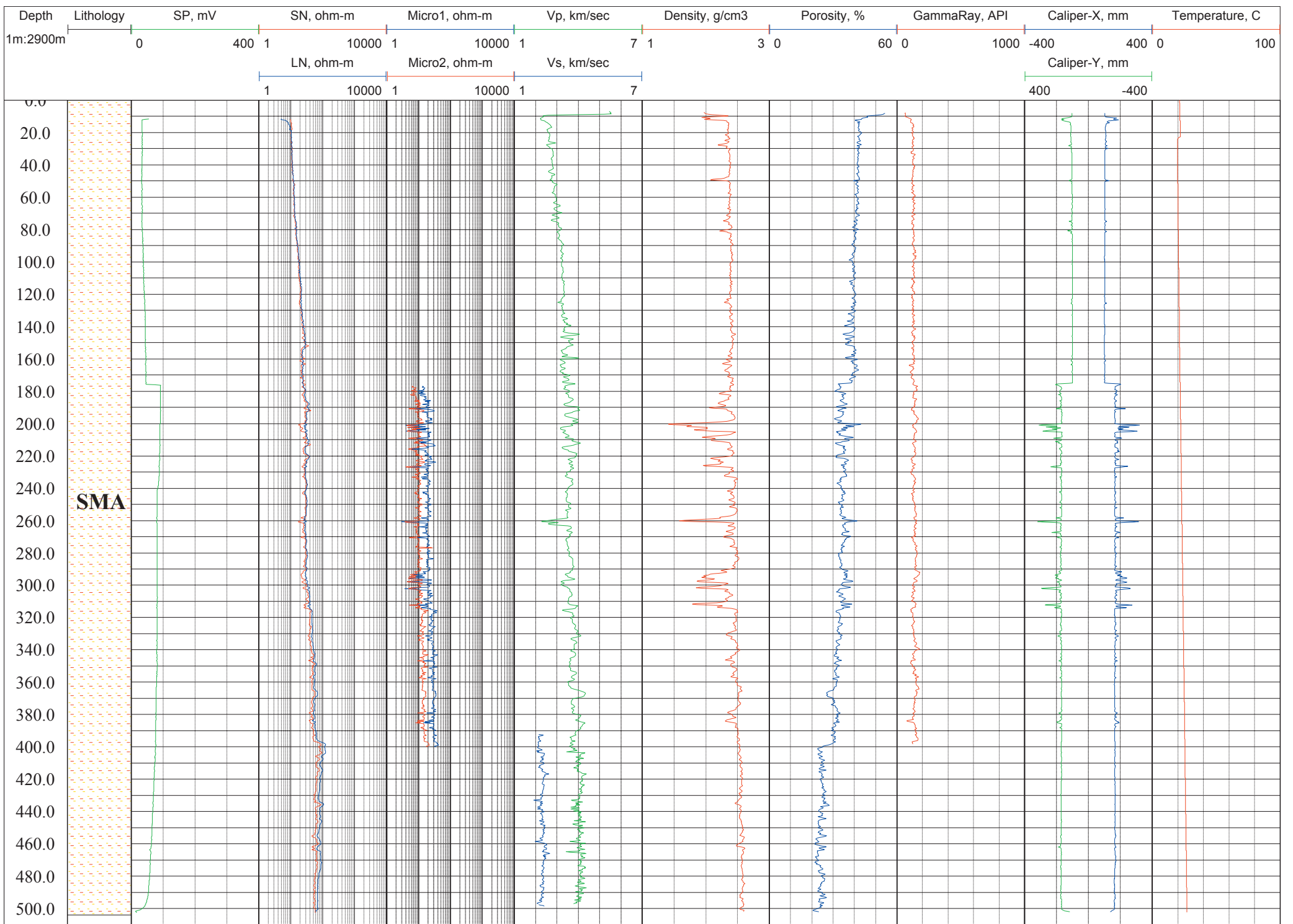


Fig. 29 Geologic column and geophysical logs for the Shingu borehole.